



ORIGINAL ARTICLE

Optimization of *Portulaca oleracea* L. extract using response surface methodology and artificial neural network and characterization of bioactive compound by high-resolution mass spectroscopy



Fanar Alshammari ^a, Md Badrul Alam ^{a,b}, Marufa Naznin ^c, Sunghwan Kim ^{c,d}, Sang-Han Lee ^{a,b,*}

^a Department of Food Science and Biotechnology, Graduate School, Kyungpook National University, Daegu 41566, Republic of Korea

^b Food and Bio-Industry Research Institute, Inner Beauty/Antiaging Center, Kyungpook National University, Daegu 41566, Republic of Korea

^c Department of Chemistry, Kyungpook National University, Daegu 41566, Republic of Korea

^d Mass Spectrometry Converging Research Center and Green-Nano Materials Research Center, Daegu 41566, Republic of Korea

Received 4 July 2022; accepted 10 November 2022

Available online 23 November 2022

KEYWORDS

Antioxidant;
Artificial neural network;
Portulaca oleracea;
Response surface methodology;
Secondary metabolites

Abstract The well-known medicinal plant *Portulaca oleracea* L. (PO) is used as a traditional medicine and culinary herb to treat various diseases. Fatty acids, essential oils, and flavonoids were extracted from PO seeds and leaves using ultrasonic, microwave, and supercritical fluid extraction with RSM techniques. However, investigations on the secondary metabolites and antioxidant capabilities of the aerial part of PO (APO) are scarce. In order to extract polyphenols and antioxidants from APO as effectively as possible, this study used heat reflux extraction (HRE), response surface methodology (RSM), and artificial neural network (ANN) modeling. It also used high-resolution mass spectrometry to identify the APO secondary metabolite. A central-composite design (CCD) was used to establish the ideal ethanol content, extraction time, and extraction temperature to extract the highest polyphenolic compounds and antioxidant activity from APO. According to RSM, the highest amount of TPC (8.23 ± 1.06 mgGAE/g), TFC (43.12 ± 1.15 mgCAE/g), DPPH-scavenging activity (43.01 ± 1.25 % of inhibition) and FRAP (35.98 ± 0.19 μ M ascorbic acid equivalent) were obtained at 60.0 % ethanol, 90.2 % time, and 50 °C. Statistical metrics such as the coefficient of determination (R^2), root-mean-square error (RMSE), absolute average deviation

* Corresponding author at: Department of Food Science and Biotechnology, Kyungpook National University, Daegu 41566, Republic of Korea. E-mail address: sang@knu.ac.kr (S.-H. Lee).

Peer review under responsibility of King Saud University.



tion (AAD), and standard error of prediction (SEP) revealed the ANN's superiority. Ninety-one (91) secondary metabolites, including phenolic, flavonoids, alkaloids, fatty acids, and terpenoids, were discovered using high-resolution mass spectrometry. In addition, 21 new phytoconstituents were identified for the first time in this plant. The results revealed a significant concentration of phytoconstituents, making it an excellent contender for the pharmaceutical and food industries.

© 2022 The Author(s). Published by Elsevier B.V. on behalf of King Saud University. This is an open access article under the CC BY-NC-ND license (<http://creativecommons.org/licenses/by-nc-nd/4.0/>).

1. Introduction

Portulaca oleracea L. (PO) is a well-known medicinal plant used both as a traditional medicine and as an edible herb to treat various ailments. This herb is widely used in European folk medicine. Additionally, PO is mentioned in some pharmacopoeias, such as the Ayurvedic Pharmacopoeia of India and the Pharmacopoeia of PR China (Iranshahy et al., 2017). Pharmacological investigations have demonstrated that PO has a wide range of biological effects, including anti-inflammatory, a bronchodilator, anti-microbial, antioxidant, and neuroprotective characteristics (Malek et al., 2004, Wang et al., 2007, Hozayen et al., 2011, Karimi et al., 2011, Du et al., 2017). Animal studies have demonstrated its hepatoprotective, antiulcerogenic, and antifertility benefits (Kumar et al., 2010, Nayaka et al., 2014, Eidi et al., 2015). Additionally, investigations on phytochemistry have revealed that this plant includes minerals, vitamins, fatty acids, flavonoids, alkaloids, and terpenoids (Sakai et al., 1996, Xiang et al., 2005, Yan et al., 2012, Petropoulos et al., 2016).

Numerous studies have demonstrated that the solvent concentration, incubation time, and temperature affect the effectiveness of polyphenol extraction, while some thermolabile bioactive substances may degrade during extraction (Saha et al., 2011). There are several extraction strategies for bioactive molecules, including reflux, soxhlet, microwave-aided, ultrasonicator-assisted, and supercritical fluid extraction (Pandey and Banik 2012). Heat reflux extraction has several benefits over more traditional extraction methods, (1) the solvent is replenished in the extraction; (2) the mass transfer driving force is more substantial, (3) the extraction takes less time, (4) the solvent is used less because it has already been used, and (5) the extraction yield is increased. This technology is a promising substitute for extracting bioactive natural compounds due to its benefits over traditional extraction methods (Gong et al., 2014, Ma et al., 2022).

Extraction is the initial and most crucial step in collecting and purifying bioactive chemicals from plant sources; yet, lengthy extraction times and low extraction efficiency limit these approaches (Samuel and Emovon 2018, Sedraoui et al., 2020). Analytical techniques were optimized using multivariate statistical methodologies to address this problem. Response surface methodology (RSM) combines mathematical and statistical methods that have proven effective in developing, improving, and optimizing complex processes (David Samuel et al., 2021). RSM provides a wealth of information and is more cost-effective because it reduces the required experiments. In addition, RSM assesses the simultaneous influence of several factors and anticipates the system's response to each new condition to find the optimal circumstances for the predicted response (Kusuma et al., 2021, Kusuma et al., 2022). Nevertheless, nonlinearity and inaccurate data are not handled precisely by RSM approaches. It has also been demonstrated that artificial neural networks (ANNs) are effective data-driven computational tools with the flexibility to capture complex and nonlinear data (Okwu et al., 2020, Okwu et al., 2021). The operation of ANN as a prediction tool is similar to that of the human brain. The brain's neurons, basic processing units connected by networks and used to transmit messages between the neurons, served as the model's primary source of inspiration. The sigmoid function controls the network (Samuel and Okwu 2019, Okwu et al., 2021, Zadhosseine et al., 2021). However, the black box learning technique associated with the ANN cannot be utilized to correlate input factors and output vari-

ables (Gupta and Sharma 2014). This problem is circumvented by incorporating an additional method, such as RSM, to analyze the interaction between the input and response variables. Hence, Combining RSM with ANN resulted in a more precise forecast (Samuel and Okwu 2019).

Mounting studies over the past few decades have shown how to extract fatty acids, essential oils, and flavonoids from PO seeds and leaves using ultrasonic, microwave, and supercritical fluid extraction with RSM methods (Stroescu et al., 2013, Wang et al., 2014, Sodeifian et al., 2018). Most of the research disclosed just process optimization. However, the authors did not compare the efficacy of predictive modeling with better methodologies, such as ANN, and there was a dearth of secondary metabolite profiling of the improved extracts. To the best of our knowledge, however, heat reflux extraction (HRE) using RSM and ANN was used for the first time in this study to increase the polyphenol content and antioxidant activity of the aerial portions of the *Portulaca oleracea* (APO). This study aimed to examine and improve extraction parameters, including extraction temperature and duration, as well as ethanol concentration, using the RSM central composite design (CCD) tool to obtain the highest polyphenolic content and antioxidant potential from APO. Additionally, for the first time, we have profiled the secondary metabolites of APO using high-resolution mass spectrometry analysis.

2. Materials and methods

2.1. Sample collection and preparation

Wild *Portulaca oleracea* L. was collected in September 2021 in Daegu, Korea. The Department of Food Science and Technology, Kyungpook National University, Daegu, Korea (voucher specimen # FT1005), identified the sample. Heat reflux extraction (HRE) was done in an oven with a condenser (Soxhlet water bath C-WBS-D6, Changshin Science, Seoul, Korea). Dry powder samples (10.0 g) were extracted using 100 ml of solvent following the instructions in supplemental Table 1. The extracted materials were filtered on Whatman No. 1 filter paper (Schleicher & Schuell, Keene, New Hampshire) and then dried in a freeze drier (II-shin Biobase, Goyang, Korea). The APO extract was kept at -20°C for the ensuing investigations.

2.2. Total phenolic content (TPC), total flavonoid content (TFC) and antioxidant activities

The TPC and TFC of APO extracts were assessed using the Folin-Ciocalteu assay and the aluminum chloride colorimetric method, respectively (Alam et al., 2017). The corresponding regression equations for the calibration curves were used to determine the TPC ($y = 0.0582x + 0.0038$; $r^2 = 0.9955$) and TFC ($y = 0.059x + 0.0081$; $r^2 = 0.9879$). The gallic acid equivalent (mg)/dry weight sample (g) and catechin equivalent (mg)/dry weight sample (g) were used as the units of measurement for the TPC and TFC, respectively. DPPH-radical scav-

Table 1 Central composite design (CCD) for independent variables and corresponding response values (experimental).

Run	Independent variables			Responses			
	(X ₁)	(X ₂)	(X ₃)	TPC (Y ₁)	TFC (Y ₂)	DPPH (Y ₃)	FRAP (Y ₄)
1	50	140	50	5.09 ± 0.68	21.20 ± 0.73	20.87 ± 0.72	19.03 ± 0.05
2	50	40	50	3.89 ± 0.83	19.42 ± 0.52	15.36 ± 0.39	16.36 ± 0.02
3	50	90	50	8.12 ± 0.34	41.89 ± 0.25	41.75 ± 0.37	35.19 ± 0.16
4	50	90	30	3.15 ± 0.26	29.07 ± 0.65	9.18 ± 0.24	12.04 ± 0.10
5	0	90	50	1.25 ± 0.41	19.76 ± 0.32	0.66 ± 1.00	3.04 ± 0.07
6	75	60	60	6.58 ± 0.82	29.09 ± 0.10	27.21 ± 0.21	26.02 ± 0.08
7	50	90	50	7.61 ± 1.02	41.75 ± 0.56	41.93 ± 0.25	35.19 ± 0.06
8	75	120	40	5.06 ± 0.49	31.02 ± 0.26	25.07 ± 0.45	23.12 ± 0.02
9	75	60	40	5.03 ± 0.42	32.02 ± 0.95	22.70 ± 0.54	22.26 ± 0.04
10	25	120	60	5.06 ± 0.23	25.75 ± 0.35	20.08 ± 0.98	17.01 ± 0.08
11	50	90	50	7.59 ± 0.62	43.20 ± 0.26	40.56 ± 0.10	35.19 ± 0.04
12	100	90	50	5.75 ± 0.06	31.50 ± 0.33	30.25 ± 1.02	25.93 ± 0.02
13	50	90	50	7.49 ± 0.04	43.02 ± 0.53	40.05 ± 0.56	35.17 ± 0.06
14	75	120	60	6.84 ± 0.08	29.02 ± 0.35	29.88 ± 0.46	27.96 ± 0.16
15	25	60	60	3.17 ± 0.06	24.52 ± 0.15	14.02 ± 0.29	15.33 ± 0.13
16	50	90	70	5.53 ± 0.24	31.01 ± 0.60	22.53 ± 0.37	21.33 ± 0.19
17	25	60	40	2.81 ± 0.68	23.13 ± 0.72	7.01 ± 0.19	10.46 ± 0.15
18	50	90	50	7.98 ± 0.68	43.11 ± 0.72	41.89 ± 0.73	35.09 ± 0.07
19	50	90	50	8.12 ± 0.83	43.23 ± 0.39	41.05 ± 0.52	36.09 ± 0.05
20	25	120	40	2.82 ± 0.34	21.03 ± 0.37	8.51 ± 0.25	9.19 ± 0.16

X₁. Ethanol concentration (%); X₂. time (min); X₃. temperature (°C); TPC. total phenolic content (mg gallic acid equivalent/g dry weight extract); TFC. total flavonoid content (mg catechin equivalent/g dry weight extract); DPPH. DPPH radical scavenging activity (% inhibition); FRAP. ferric reducing antioxidant power (μM ascorbic acid equivalent).

enging test and ferric reducing antioxidant power (FRAP) assay were used to assess the antioxidant properties of APO extracts (Alam et al., 2021).

2.3. RSM design and extraction process

The RSM model was designed to extract phenolic chemicals from APO using ethanol concentration (X₁), extraction duration (X₂), and temperature (X₃) as independent process factors. Respondent factors included TPC, TFC, DPPH-scavenging activity and FRAP (Y₁-Y₄, respectively). A three-component, five-layer CCD was employed for the extractions (supplementary data Table S1). The CCD is widely utilized due to its adaptability. The early experimental results from a factorial design can be used in a CCD that only makes the axial points, eliminating resource waste. Nonetheless, the most distinctive parameters are the axial points ($-\alpha$, α). These locations are outside the minimum and maximum limits of the factors, guaranteeing the response surface's curvature and allowing the construction of ideal conditions. In contrast to the BBD, a CCD can distinguish between axial point estimates based on orthogonal and rotational characteristics. An orthogonal design allows for an independent examination of the primary, interaction, and quadratic effects, simplifying the interpretation of the results. The second-order polynomial model equation (Eq.1) describes the link between independent factors and replies.

$$Y = \beta_0 + \sum_{i=1}^n \beta_i X_i + \sum_{i=1}^n \beta_{ii} X_i^2 + \sum_{i=1}^{n-1} \sum_{j=i+1}^n \beta_{ij} X_i X_j \quad (1)$$

where Y, X_i and X_j as well as β_0 represents the response variable, independent coded variables and the constant coefficient, respectively, while β_i , β_{ii} , and β_{ij} represent the coefficients of linear, quadratic, and interaction effects, respectively.

The model's adequacy was assessed using the determination coefficient (R²), the adjusted determination coefficient (Adj. R²), and the lack of fit test. The F-value ($p < 0.05$) was significant. Three-dimensional (3D) surface plots showed each factor's effect on response value. The RSM analysis and multiple linear regression were carried out using Design Expert 11 (Stat-Ease, Minneapolis, Minnesota, USA).

2.4. Artificial neural networks (ANN) modeling

The ANN modelling was systematically conducted by using the dataset presented in Table 1. MATLAB R2020a software (The Neural Network Toolbox, Inc., USA) was employed to create the ANN model. The ANN design consists of data collection; model development using different functions and algorithms; configuration of the model; weights and biases initialization; training, testing, and validation of the model. The MLP (multilayer perceptron network) topology consists of input, hidden, and output layers. Independent variables (X₁, X₂, and X₃) were used as input vectors, and four responses (Y₁, Y₂, Y₃, and Y₄) were applied as target vectors (Fig. 1A). The data were divided into three subsets, where 70, 15, and 15 % of the whole data points were utilized for training, validation, and testing, respectively. In the training step, the feed-forward network and cascade feed-forward network with the Broyden-Fletcher-Goldfarb-Shanno algorithm (BFGS) and Levenberg-Marquardt back-propagation algo-

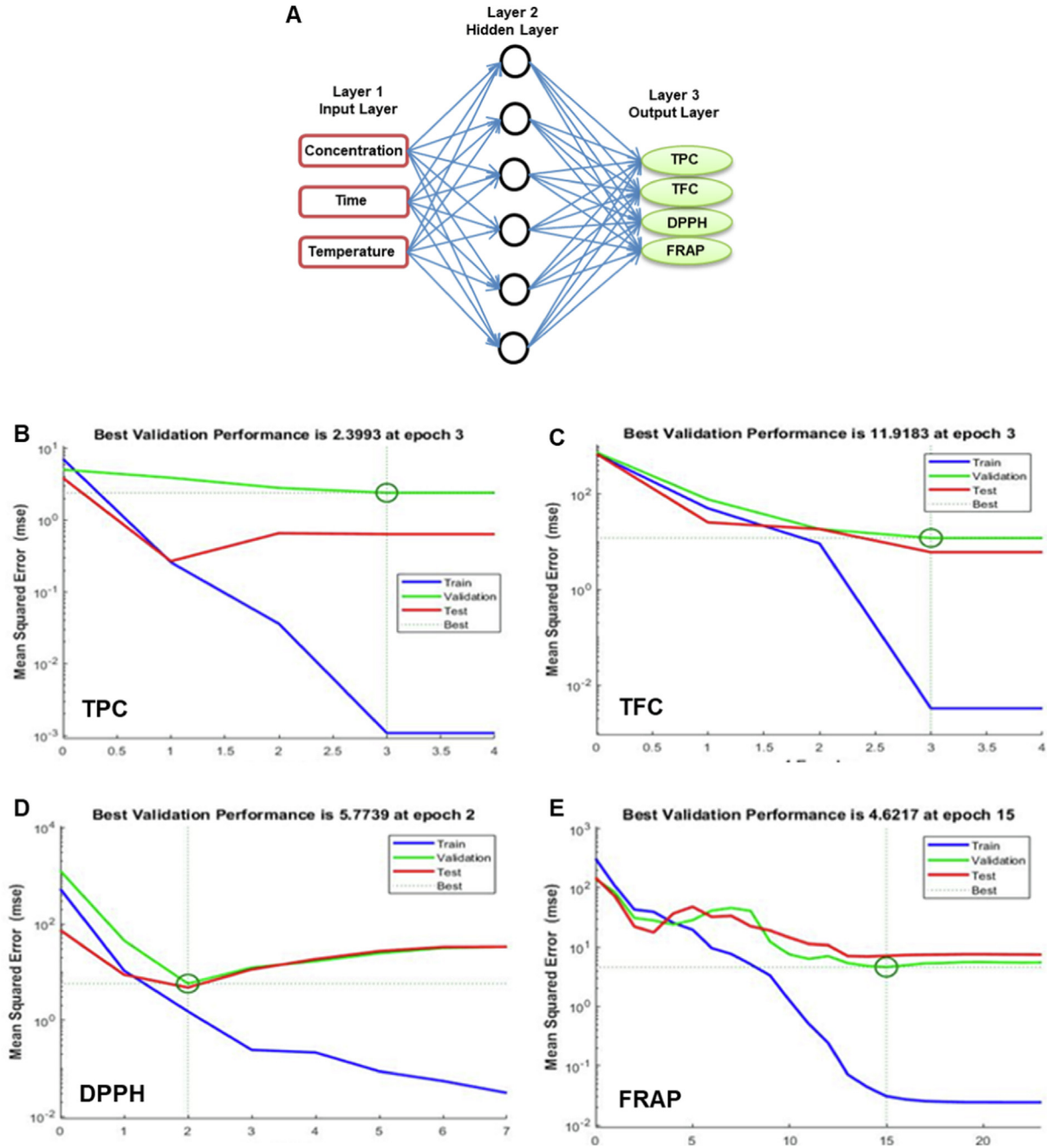


Fig. 1 ANN model topology. The best ANN model in terms of architecture (A), network training curves for trained subsets with epoch numbers for TPC (B), TFC (C), DPPH (D) and FRAP (E) using the MATLAB software.

rithm were used to lessen the mean square error (MSE). The MSE was calculated using Eq. (2)

$$MSE = \frac{1}{N} \sum_{i=1}^N (Y_{ANN} - Y_{Exp})^2 \quad (2)$$

where Y_{Exp} is the experimental outcomes, N represents to sample number and Y_{ANN} is the predicted value. A hyperbolic tangent sigmoid transfer function was used for pattern recognition and network modeling using Eq. (3)

$$f(x) = \text{tansig}(n) = \frac{2}{1 + e^{-2x}} - 1 \quad (3)$$

2.5. Comparison of the RSM and ANN models' predictive abilities

To evaluate the estimation skills of RSM and ANN, several statistical metrics such as R^2 , RMSE, AAD, and SEP were calculated using the following equations.

$$R^2 = 1 - \frac{\sum_{i=1}^n (Y_p - Y_e)^2}{\sum_{i=1}^n (Y_m - Y_e)^2} \quad (4)$$

$$RMSE = \sqrt{\frac{\sum_{i=1}^n (Y_p - Y_e)^2}{n}} \quad (5)$$

$$AAD = \left[\frac{\sum_{i=1}^n (|Y_p - Y_e|/Y_e)}{n} \right] \times 100 \quad (6)$$

$$SEP = \frac{RMSE}{Y_m} \times 100 \quad (7)$$

where Y_p is the predicted response; Y_e is the observed response; Y_m is the average response variable; n is the number of experiments.

2.6. Model validation

The optimal extraction parameters were determined using response surface and desirability function analysis. A series of three experiments was conducted under ideal conditions to ensure the model's accuracy, with the average experimental results compared to predictions. In addition, the electrospray ionization mass spectrometry (ESI-MS)/MS profiles of bioactive compounds were identified under optimum conditions.

2.7. Identification of bioactive compounds by ESI-MS/MS analysis

The negative (-) mode ESI-MS was performed on a Q-Exactive Orbitrap mass spectrometer (Thermo Fisher Scientific Inc., San Jose, CA, USA). Immersing the sample in the ESI source required a 500 L graded syringe (Hamilton Company Inc., Reno, NV, USA) and a 15 L/min syringe pump (Model 11, Harvard, Holliston, MA, USA). The normal negative mode ESI-MS conditions were as follows: mass resolution of 140,000 (full width at half maximum, FWHM), sheath gas flow rate of 5, seep gas flow rate of 0, auxiliary gas flow rate of 0, spray voltage of 4.20 kV, capillary temperature of 320 °C, S-lens Rf level, and automatic gain control of 5 E 6. The MS/MS investigations used the same apparatus with three stepwise normalized collision energies (10, 20, and 30) (Alam et al., 2021). Mass spectrum data was processed using the Xcalibur 3.1 with Foundation 3.1 (Thermo Fisher Scientific Inc., Rockford, IL, USA). The compounds were probably found by comparing the calculated (exact) masses of deprotonated (M-H) adducts with the m/z values and ESI-MS/MS fragmentation patterns from the in-house MS/MS database and online databases like FooDB (Naveja et al., 2018), METLIN (Guijas et al., 2018), CFM-ID 4.0 (Wang et al., 2021). The ChemDraw Professional 15.0 (PerkinElmer, Waltham, MA, USA) was used to draw the chemical structure.

2.8. Statistical analysis

All data were reported as the mean \pm standard deviation of at least three independent experiments ($n = 3$), each with three sample replicates. Differences were considered significant at $p < 0.001$, $p < 0.01$, and $p < 0.05$.

3. Results and discussion

3.1. Fitting of the RSM and ANN models

For each extraction circumstance, Table 1 describes the experimental settings and conclusions. All response variables were transformed into second-order quadratic polynomial equa-

tions to account for changes in answers as a function of extraction factors. ANOVA was used to determine whether the fitted second-order quadratic model equations were statistically significant. The regression coefficient (β), adjusted correlation factor (R^2), coefficient of variation (CV), and adequate precision were used to describe how well the model fit (Table 2). The nonsignificant terms ($p > 0.05$) were taken out of the models to improve the fit and predictions. We used the p -values to figure out how vital each coefficient was. When the p -values were < 0.05 , 0.01 , and 0.001 , the model terms were significant, very significant, and strikingly significant, respectively.

Table 2 shows that model terms are significant ($p < 0.0001$). The R^2 values (0.9892–0.9988) of the built regression models indicate a high level of statistical significance. The appropriate precision indicates a signal-to-noise ratio, and > 4 is ideal (Alam et al., 2022). The ratio ranged between 31.55 and 93.26, showing a significant signal and suitability for this method. The coefficient of variation (CV) measures the repeatability of a model, and the range of 2.14 to 5.47 indicates that the model is reproducible. Multiple linear regression equations were used to create 3D surfaces and contour plots to show independent variable interactions (Fig. 2A-D).

Mounting evidence revealed that ANN modeling is superior and more sophisticated than RSM, and ANNs are a feasible alternative to RSM for complicated nonlinear multivariate modeling. ANNs are more exact than RSM at fitting experimental responses, predicting, and modeling biological processes (Huang et al., 2017). ANN modeling was used to verify the experimental values. The trained ANN model's predicted values are in Table S2. The ANN predicts nonlinear relationships between extraction parameters (X_1 , X_2 , and X_3) and response variables (Y_1 , Y_2 , Y_3 , and Y_4). The ANN model predicted values that were pretty close to the actual values, proving its accuracy. By comparing network training and testing errors, the hit-and-try strategy modified the number of hidden layer neurons. The experiment investigated the lowest practicable error between training and testing and the minimal number of epochs to prevent model overfitting; the results were consistent with earlier efforts (Choi et al., 2022). The Levenberg-Marquardt approach produced the best validation result for all dependent variables Y_1 , Y_2 , Y_3 , and Y_4 (Fig. 1B-E).

3.2. Comparison of the RSM and ANN models' predictive abilities

Both the RSM and ANN models' prediction and estimation skills were examined. Comparative similarity plots were utilized to examine the ANN model's four target response predictions (Y_1 , Y_2 , Y_3 , and Y_4). In terms of fitting experimental data to all target responses, the ANN model was more accurate, precise, and assessable than the RSM model (supplementary data Table S2). The RSM model had a larger discrepancy between projected and actual data, whereas the ANN model's residuals remained steady.

To compare RSM with ANN, R^2 , RMSE, AAD, and SEP were calculated (Table 3). A better model has lower RMSE, AAD, and SEP while higher R^2 . R^2 values of the trained ANN model were greater than those of the RSM model, suggesting the ANN model's superiority in predicting all four

Table 2 (continued)

ANOVA for quadratic model for TPC							
Source	RC	SS	DF	MS	F-value	p-value	
ANOVA for quadratic model for FRAP							
Model		1975.64	9	219.52	900.96	< 0.0001	Significant
Intercept	35.30						
Linear terms							
X ₁	5.82	542.31	1	542.31	2225.80	< 0.0001	Significant
X ₂	0.5651	4.33	1	4.33	17.77	0.0018	Significant
X ₃	2.49	99.35	1	99.35	407.77	< 0.0001	Significant
Interaction terms							
X ₁ X ₂	0.2988	0.7140	1	0.7140	2.93	0.1177	
X ₁ X ₃	-0.5112	2.09	1	2.09	8.58	0.0151	Significant
X ₂ X ₃	0.5038	2.03	1	2.03	8.33	0.0162	Significant
Quadratic terms							
X ₁ ²	-5.23	698.20	1	698.20	2865.65	< 0.0001	Significant
X ₂ ²	-6.39	551.56	1	551.56	2263.76	< 0.0001	Significant
X ₃ ²	-4.68	559.01	1	559.01	2294.37	< 0.0001	Significant
Lack of Fit		1.72	5	0.3435	2.39	0.1806	Non-significant
Pure error		0.7190	5	0.1438			
R ²							0.9988
Adjusted R ²							0.9977
Adeq Precision							93.2690
C.V. %							2.14

RC. Regression coefficient; SS. sum of squares; MS. mean square.

dependent variables. The AAD gauges the deviation between projected and actual data, while RMSE shows model fit. The ANN outperformed RSM by having lower AAD and RMSE values. The ANN model also showed low SEP values, which ranged from 0.0813 to 0.3126. The ANN model is more predictive than the RSM model because it can approximate nonlinear systems, while the RSM model requires second-order polynomial regression. The ANN model is also unaffected by experimental design and calculates several replies in a single run, while the RSM model takes multiple runs for multi-response optimization (Dadgar et al., 2015).

3.3. Influence of HRE parameters on TPC and TFC

In APO extracts, TPC and TFC contents ranged from 1.25 ± 0.41 to 8.12 ± 0.34 mgGAE/g and 19.76 ± 0.32 to 43.23 ± 0.91 mgCAE/g, respectively (Table 1). Both the TPC and TFC exhibited a substantial linear influence of X₁ and the quadratic component of (X₁²), (X₂²), and (X₃²) (supplementary data Figure S1). The second-order polynomial equations in eqs. (8) and (9) illustrate the relationships between TPC, TFC, and their variables.

$$\begin{aligned}
 TPC(Y_1) = & 7.82 + 1.17X_1 + 0.3091X_2 + 0.6681X_3 \\
 & - 1.08X_1^2 - 1.20X_2^2 - 0.8696X_3^2 \\
 & - 0.2012X_1X_2 + 0.0912X_1X_3 + 0.2637X_2X_3 \quad (8)
 \end{aligned}$$

$$\begin{aligned}
 TFC(Y_2) = & 42.67 + 3.14X_1 + 0.0757X_2 + 0.2375X_3 \\
 & - 4.30X_1^2 - 8.14X_2^2 - 3.12X_3^2 - 0.0250X_1X_2 \\
 & - 1.38X_1X_3 + 0.5325X_2X_3 \quad (9)
 \end{aligned}$$

The TPC and TFC showed nonsignificant lack of fit values ($F = 1.16$ and 1.67 , respectively) showing the model accurately predicted $R^2 = 0.9892$ (TPC) and 0.9956 (TFC) and Adj. $R^2 = 0.9795$ (TPC) and 0.9949 (TFC) (Table 2). The RSM model accurately predicted the parameter impacts on TPC and TFC of the APO extract. As depicted in Fig. 2(A, B), at 50 °C, 50 % ethanol produced the most TPC and TFC in 90 min. Previous studies revealed that medium-concentration ethanol may make the solvent more polar, dissolving more polar and moderately polar phenolic compounds (Sedraoui et al., 2020). Moderate ethanol in water can affect the architecture and structure of membrane phospholipids. This affects plant cell penetrability, allowing higher polyphenol extraction and diffusion (Gurtovenko and Anwar 2009). Experiments in a prior comparison investigation found that extraction of phenolic compounds from green tea leaves under high hydrostatic pressure increased with ethanol in the solvent; peaked at 50 % ethanol and fell after that (Xi and Wang 2013).

3.4. Effect of HRE parameters on the in vitro antioxidant capacity (AC)

A linear significant influence of ethanol content (X₁), a quadratic effect of concentration (X₁), time (X₂) and temperature (X₃) as well as interaction between concentration and temperature (X₁X₃) (supplementary data Figure S1) on antioxidant activity were found using DPPH radical scavenging activity and FRAP analyses. Eqs. (10) and (11) display the fitted second-order polynomial equations for DPPH (% inhibition) and FRAP (ascorbic acid equivalent μM):

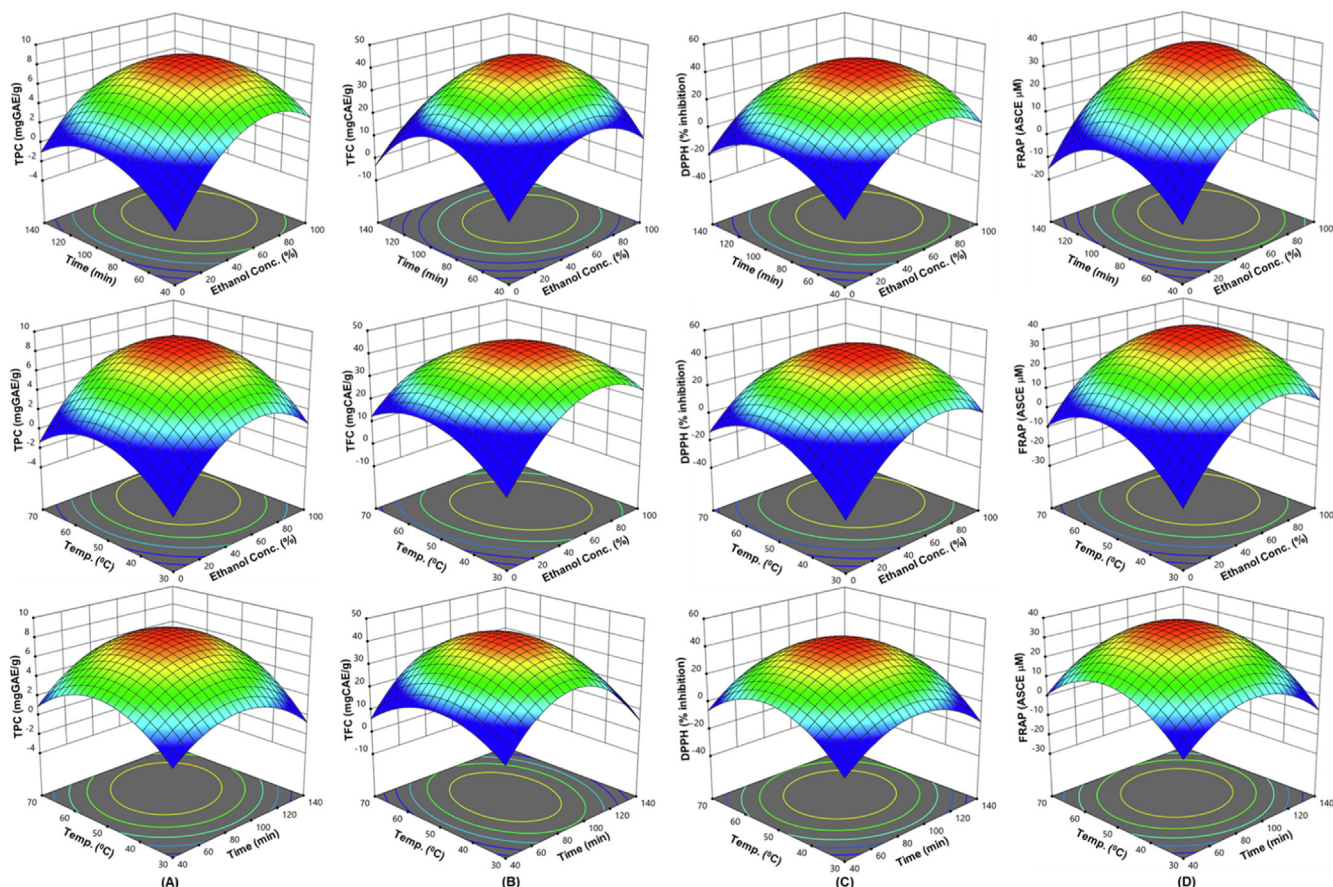


Fig. 2 The three-dimensional (3D) response surface plots of APO extraction for TPC (A), TFC (B), DPPH-radical scavenging activity (C), and FRAP (D) for ethanol concentration, time, and temperature as a function of key interaction factors for RSM.

Table 3 Comparison of the prediction abilities of the RSM and ANN models.

Parameters	TPC		TFC		DPPH		FRAP	
	RSM	ANN	RSM	ANN	RSM	ANN	RSM	ANN
R ²	0.9892	0.9976	0.9956	0.9997	0.9973	0.9985	0.9988	0.9995
RMSE	0.1299	0.0753	2.3413	1.7888	1.6655	1.0867	1.3608	1.1492
AAD (%)	2.2909	1.1408	6.6496	3.0372	28.8295	14.4468	4.9237	3.1221
SEP (%)	0.1401	0.0813	0.4091	0.3126	0.4675	0.3050	0.3567	0.3012

R². correlation coefficient; RMSE. root-mean-square error; AAD. absolute average deviation; SEP. standard error of prediction.

$$\begin{aligned}
 DPPH(Y_3) = & 41.13 + 7.15X_1 + 1.61X_2 + 3.41X_3 \\
 & - 6.52X_1^2 - 8.49X_2^2 - 6.42X_3^2 \\
 & - 0.3150X_1X_2 - 1.16X_1X_3 + 0.6075X_2X_3 \quad (10)
 \end{aligned}$$

$$\begin{aligned}
 FRAP(Y_4) = & 35.30 + 5.82X_1 + 0.5651X_2 + 2.49X_3 \\
 & - 5.23X_1^2 - 6.39X_2^2 - 4.68X_3^2 \\
 & + 0.2988X_1X_2 - 0.5112X_1X_3 \\
 & + 0.5038X_2X_3 \quad (11)
 \end{aligned}$$

The AC values ranged from 0.66 ± 1.00 % to 41.89 ± 0.22 % inhibition of DPPH and from 3.04 ± 0.07 to 36.09 ± 0.34 μ M ascorbic acid equivalent (Table 1). The ANOVA

results show that the data fitted the model results for DPPH ($R^2 = 0.9973$ and $Adj. R^2 = 0.9949$) and FRAP response ($R^2 = 0.9988$ and $Adj. R^2 = 0.9977$), and the lack of fit was nonsignificant ($F = 1.92$ for DPPH and 2.39 for FRAP) (Table 2). As depicted in Fig. 2(C, D), at 50 $^{\circ}$ C, 50 % ethanol produced the highest DPPH inhibition and FRAP value in 90 min. This indicates that the capacity for electron and proton donation improves with increasing amounts of the organic solvent. This outcome is in line with the earlier discovery for TFC that maximum extraction calls for 75 percent ethanol (Do et al., 2014). The extraction of considerable polyphenolics from APO, both in terms of quality and quantity, is made possible by raising the ethanol concentration. There is growing

evidence that ethanol concentrations affect antioxidant activity and polyphenolic compound quality and amount (Zhu et al., 2011, Do et al., 2014).

3.5. Model validation

The desirability function optimizes TPC, TFC, DPPH, and FRAP simultaneously. Derringer's desirability function was used to anticipate the parameters, allowing a multivariate analysis to find the best level for all replies in a single extraction. In this study, the following conditions (X_1 : 60 %), (X_2 : 90.5 min), and (X_3 : 50 °C), was used to achieve the maximal overall desirability $D = 0.999$ (on a scale of 0 to 1). Under these optimal conditions, the predicted values for TPC, TFC, percentage inhibition of DPPH, and μM ascorbic acid equivalent FRAP are 8.12 mgGAE/g, 43.23 mgCAE/g, and 42.98 %, and 36.81, respectively. To verify the sufficiency of the model equations, a duplicate experiment was conducted in the optimal conditions predicted by Derringer's desire model. The following results were obtained: TPC = 8.23 ± 1.06 mgGAE/g, TFC = 43.12 ± 1.15 mgCAE/g, % inhibition of DPPH = 43.01 ± 1.25 %, and μM ascorbic acid equivalent FRAP = 35.98 ± 0.19 . The model efficiently optimized the common extraction parameters for all responses, as evidenced by the good agreement between experimental and expected values (supplementary data Table S3).

Additionally, comparison research between this study and earlier studies was carried out to confirm the high extractability of hydro-alcoholic solvents for polyphenols and the antioxidant properties of APO. The hydro-alcoholic solvent had more TPC and DPPH scavenging action than other solvents, as indicated in Table 4. When compared to alternative solvents, which were typically utilized in earlier studies, these comparisons showed that the HRE technique using hydro-alcoholic solvent was a high-efficiency technique.

3.6. Identification of secondary metabolites in APO by high-resolution mass spectroscopy

The ESI-MS/MS in negative ionization techniques detected secondary metabolites in APO extracts. Table 4 shows that 93 compounds were identified in negative mode utilizing MSn data from the precursor ion mass, fragments, recognized fragmentation patterns for the provided classes of compounds, and neutral mass loss, as well as literature and online database searches. The confidence level determined the significance of these results. Level 2 shows the likely structure of the detected substance, whereas Level 3 denotes a speculative candidate. (Schymanski et al., 2014).

3.6.1. Phenolic acids

A phenolic acid can lose methyl (15 Da), hydroxyl (18 Da), or carboxyl (44 Da) to form a fragment ion. Fragmentation of a phenolic acid glycoside begins with cleavage of the glycosidic bond to give phenolic acid m/z and sugar loss (neutral mass loss of 162 Da) (Choi et al., 2022). In addition, hydroxycinnamic acid conjugates yield quinate (m/z 191) by loss of the acyl group and dehydrated quinate (m/z 173), coumarate (m/z 163), caffeate (m/z 179), ferulate (m/z 193) and sinapate (m/z 223) through β -elimination of a carboxylic acid (Jaiswal et al., 2010, Parveen et al., 2011). Thus, compounds 1–3, 5,

7, 8, 10–16, and 20 were tentatively identified as hydroxy benzoic acid, coumaric acid, ferulic acid, caffeic acid phenethyl ester, ellagic acid, protocatechuic acid glucoside, coumaroylquinic acid, caffeic acid hexoside, ferulylshikimic acid, ferulic acid hexoside, syringoylquinic acid, caffeic acid derivatives, feruloyl galactaric acid and hexosyl caffeoyl hexose (Islam et al., 2020, Alam et al., 2021, Fernández-Poyatos et al., 2021, Choi et al., 2022). In addition, by comparing the fragmentation patterns to those previously published in the literature, compound 4, 6, 17, 18 and 21 was identified as maclurin ($\text{C}_{13}\text{H}_{10}\text{O}_6$), uralennoiside ($\text{C}_{12}\text{H}_{14}\text{O}_8$), picraquassioside A ($\text{C}_{18}\text{H}_{22}\text{O}_{10}$), methylpicraquassioside A ($\text{C}_{19}\text{H}_{24}\text{O}_{10}$) and aril-latose B ($\text{C}_{22}\text{H}_{29}\text{O}_{14}$), respectively which yielded a precursor ion $[\text{M}-\text{H}]$ at m/z 261.0401, 285.0612, 397.1142, 411.1302, and 517.1563, respectively (Berardini et al., 2004, Abdelrahman et al., 2017, Llorach et al., 2019, Tang et al., 2020). All of these substances were intriguingly discovered for the first time in APO. Furthermore, compound 9 generated a monoisotopic ion $[\text{M}-\text{H}]$ at m/z 333.0618 and produced fragment ions at m/z 289.07 by loss of carboxyl (-44 Da) group and at m/z 271.06 through successive loss of H_2O . It also yielded a characteristic ion at m/z 167.03 by cleavage of ether bond between C7-C9 and tentatively confirmed as bercloneic acid B, which has been identified as first time in APO (Fig. 3A). In addition, compound 19 was tentatively identified as paederol B with molecular formula ($\text{C}_{20}\text{H}_{28}\text{O}_{12}$), generated a deprotonated ion at m/z 459.1511 and yielded the following fragment ions: m/z at 399.12 ($[\text{M}-\text{H}-61 \text{ Da}]$), 341.08 ($[\text{M}-\text{H}-\text{C}_4\text{H}_{10}\text{O}_3-\text{CH}_3]$), 281.08 ($[\text{M}-\text{H}-178 \text{ Da}]$) and 193.05 (ferulate ion) through β -elimination of a carboxylic acid (Fig. 3B). This compound has also been first time identified in APO.

3.6.2. Flavonoids

According to a prior study, each subgroup of flavonoids exhibits a distinct fragmentation pattern during mass analysis. The most common fragmentation of flavonoids is the cleavage of the C-ring bonds (*retro*-Diels-Alder, i.e., RDA mechanism), which forms ions with the A- or B-ring and a portion of the C-ring. There may also be significant losses of tiny neutral molecules, such as CO (28 Da), $\text{C}_2\text{H}_2\text{O}$ (42 Da), COO (44 Da), 2CO (56 Da), CO + COO (72 Da), and 3CO (84 Da). A unique ion $[\text{M}-\text{H}-\text{CH}_3]$, distinguished by the loss of 15 Da, is also present in methylated flavonoids (Alam et al., 2021, Choi et al., 2022). Flavonoids typically undergo glycosylation. *O*-glycosides, *C*-glycosides, and *O-C*-glycosides are formed when the glycoside residues are connected to the *O* and *C* atoms of the flavonoids. Hexoses (162 Da), deoxyhexoses (146 Da), pentoses (132 Da), and an aglycone ion are the neutral species that result from the usual fragmentation of *O*-glycosides. As opposed to this, *C*-glucosides result in a series of fragments due to the cleavage of the C-C bonds with the sugar moiety. Some examples of these fragments include $[\text{M}-\text{H}-60]^-$, $[\text{M}-\text{H}-90]^-$, and $[\text{M}-\text{H}-120]^-$, which are used as the distinctive diagnostic ions of glycone (Vukics and Guttman 2010, Kachlicki et al., 2016). Compounds 22–29 were identified as eriodictyol, catechin, dactylorhin C, taxifolin-7-sulfate, diadzin, cajanone, phenethylrutinoside, and kaempferol glucoside respectively, based on the similarities noticed in their fragmentation behaviors and the behaviors mentioned

Table 4 Comparative study of the polyphenolic content and antioxidant activity of APO with prior study report.

Methods	Solvent	TPC (mgGAE/g)	DPPH IC ₅₀ (mg/ml)	Ref.
HRE	HM	8.23	1.01	Present study
HRE	M	4.78	1.78	
HRE	M	6.98	2.52	
HRE	E	3.60	3.56	
HRE	W	4.41	2.35	

HM. 60% methanol; M. 100% methanol; E. 100% ethanol and W. 100% aqueous solvent.

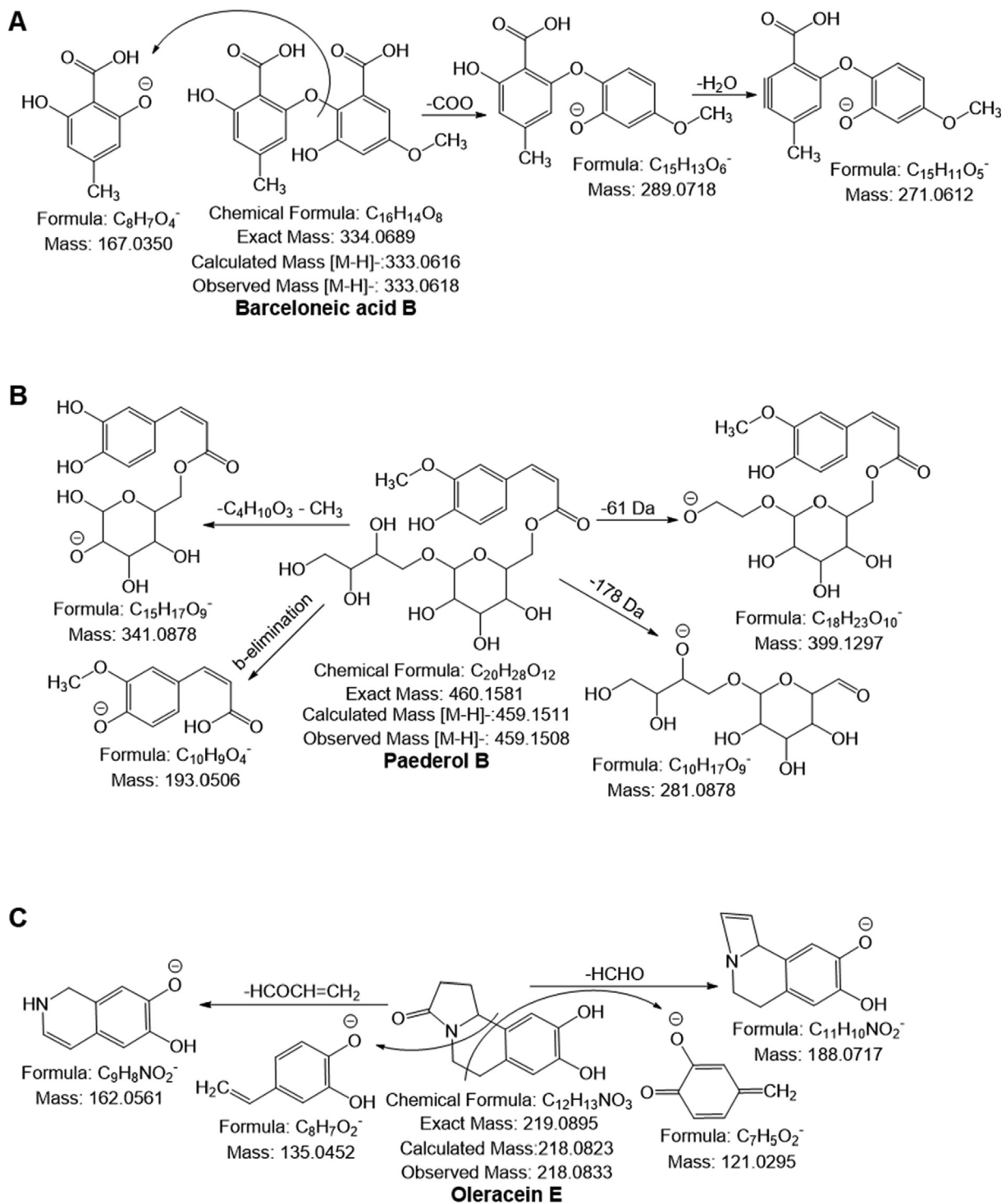


Fig. 3 Possible mass fragmentation pattern of (A) barceloneic acid B, (B) paederol B and (C) Oleracein E.

Table 5 List of possible identified compounds of the optimized extract of *Potulaca oleracea* by ESI-MS/MS.

	No.	Compound name	EF	OM (<i>m/z</i>) ⁻	CM (<i>m/z</i>) ⁻	MS/MS (negative mode)	CL
Phenolic acid	1	4-Hydroxy benzoic acid	C ₇ H ₆ O ₃	137.0253	137.0244	119.03, 93.01	2
	2	Coumaric acid	C ₉ H ₈ O ₃	163.0402	163.0401	119.04,	2
	3	Ferulic acid	C ₁₀ H ₁₀ O ₄	193.0521	193.0506	179.03, 149.06, 135.04	2
	4	Maclurin#	C ₁₃ H ₁₀ O ₆	261.0401	261.0405	151.00, 107.01	3
	5	Caffeic acid phenethyl ester	C ₁₇ H ₁₆ O ₄	283.0967	283.097	265.08, 239.07, 179.03, 163.04, 135.04	3
	6	Uralennoiside#	C ₁₂ H ₁₄ O ₈	285.0612	285.0616	153.01, 109.02	3
	7	Ellagic acid	C ₁₄ H ₆ O ₈	300.9893	300.9984	283.99, 245.00, 229.01, 200.01, 185.02	2
	8	Protocatechuic acid glucoside	C ₁₃ H ₁₆ O ₉	315.072	315.0716	162.02, 153.01	2
	9	Barceloneic acid B#	C ₁₆ H ₁₄ O ₈	333.0618	333.0618	289.07, 271.06, 167.03	3
	10	Coumaroylquinic acid	C ₁₆ H ₁₈ O ₈	337.0924	337.0626	191.05, 163.03	2
	11	Caffeic acid hexoside	C ₁₅ H ₁₈ O ₉	341.1084	341.0872	215.03, 179.06, 161.04, 135.04	2
	12	Ferulyshikimic acid	C ₁₇ H ₁₈ O ₈	349.0927	349.0923	193.05, 177.01, 173.04, 155.03, 129.02	2
	13	Ferulic acid hexoside	C ₁₅ H ₁₆ O ₁₀	355.0666	355.0665	193.05, 179.02, 149.05, 134.02	2
	14	Syringoylquinic acid	C ₁₆ H ₂₀ O ₁₀	371.0981	371.0978	353.08, 191.05, 173.04, 135.04	2
	15	caffeic acid derivatives	C ₁₈ H ₁₈ O ₉	377.0885	377.0878	341.11, 215.03, 179.05, 161.03	2
	16	Feruloyl-galactaric acid	C ₁₆ H ₁₈ O ₁₁	385.0828	385.0776	341.08, 209.03, 191.03, 147.02	2
	17	Picraquassioside A#	C ₁₈ H ₂₂ O ₁₀	397.1142	397.1135	235.06, 217.05, 191.07, 187.04, 177.05	3
	18	Methylpicraquassioside A#	C ₁₉ H ₂₄ O ₁₀	411.1302	411.1297	397.11, 249.07, 231.06, 219.06, 201.05	3
	19	Paederol B#	C ₂₀ H ₂₈ O ₁₂	459.1511	459.1508	399.12, 341.12, 281.10, 193.05	3
	20	Hexosyl caffeoyl hexose	C ₂₁ H ₂₈ O ₁₄	503.1393	503.1401	341.0.08, 179.03, 161.02	2
	Flavonoids	21	Arillatose B#	C ₂₂ H ₂₉ O ₁₄	517.1563	517.1557	313.05, 193.05
22		Eriodictyol	C ₁₅ H ₁₂ O ₆	287.0565	287.0555	179.01, 151.00, 135.04, 125.01, 107.03	2
23		Catechin	C ₁₅ H ₁₄ O ₇	289.0721	289.0712	245.08, 205.05, 179.03, 135.04	2
24		Dactylorhin C	C ₁₄ H ₂₄ O ₁₀	351.1293	351.1291	189.07, 179.05, 171.06, 163.06, 127.07	2
25		Taxifolin-7-sulfate	C ₁₅ H ₁₂ O ₁₀ S	383.0105	383.0079	303.05, 285.04, 275.05, 151.00, 125.03	2
26		Daidzin	C ₂₁ H ₂₀ O ₉	415.1029	415.1035	253.05, 235.04, 225.02, 135.00, 119.05	2
27		Cajanone	C ₂₅ H ₂₆ O ₆	421.1662	421.1651	383.12, 217.05, 197.09, 165.07, 151.00	2
28		Phenethylrutinoside	C ₂₀ H ₃₀ O ₁₀	429.1767	429.1761	249.09, 205.01, 161.04, 145.05, 119.05,	2
29		Kaempferol-3-O-glucoside	C ₂₁ H ₂₀ O ₁₁	447.0932	447.0928	285.04, 271.06, 256.02, 240.04, 151.00	2
Alkaloids		30	Oleracein E	C ₁₂ H ₁₃ NO ₃	218.0833	218.0823	200.07, 190.08, 160.04, 121.02
	31	Feruloyltyramine	C ₁₂ H ₁₃ NO ₅	250.0724	250.0721	206.08, 191.07, 177.05, 149.06	2
	32	Coumaroyltyramine	C ₁₇ H ₁₇ NO ₃	282.1128	282.1123	279.01, 162.03, 145.03, 134.02, 119.02	2
	33	Caffeoyltyramine	C ₁₇ H ₁₇ NO ₄	298.1085	298.1079	280.09, 178.05, 160.04, 136.07, 121.06	2
	34	Feruloyltyramine	C ₁₈ H ₁₉ NO ₄	312.1235	312.1241	177.05, 149.06, 136.07, 121.06, 119.05	2
	35	Feruloyloctopamine	C ₁₈ H ₁₉ NO ₅	328.1181	328.1184	310.02, 161.05, 133.02	2
	36	Oleracein U	C ₁₈ H ₁₅ NO ₆	340.0831	340.0827	322.07, 296.09, 194.04, 145.02, 132.04	2

(continued on next page)

Table 5 (continued)

	No.	Compound name	EF	OM (<i>m/z</i>) ⁻	CM (<i>m/z</i>) ⁻	MS/MS (negative mode)	CL
	37	Oleracein A	C ₂₄ H ₂₅ NO ₁₁	502.1351	502.1349	340.08, 296.09, 194.05, 145.02	2
	38	Oleracein B	C ₂₅ H ₂₇ NO ₁₂	532.1463	532.1455	370.09, 326.10, 194.05, 175.04, 161.02	2
	39	Oleracein C	C ₃₀ H ₃₅ NO ₁₆	664.1883	664.1877	502.13, 340.08, 296.09, 194.04, 145.02	2
	40	Oleracein I	C ₃₁ H ₃₇ NO ₁₇	694.1989	694.1983	518.15, 370.09, 326.10, 194.04, 175.04	2
	41	Oleracein P	C ₃₆ H ₄₅ NO ₂₁	826.2395	826.2405	664.18, 502.13, 340.08, 194.04, 145.02	2
	42	Oleracein N/S	C ₄₀ H ₄₃ NO ₁₉	840.2336	840.2351	694.19, 664.18, 340.08, 194.04, 145.02	2
	43	Oleracein L/J	C ₄₀ H ₄₃ NO ₂₀	856.2276	856.2300	694.19, 518.15, 326.10, 194.04, 161.02	2
	44	Oleracein O	C ₄₁ H ₄₅ NO ₂₀	870.2443	870.2456	694.19, 518.15, 194.04, 175.04, 161.02	2
Fatty acids	45	Citramalic acid	C ₅ H ₈ O ₅	147.0319	147.0299	129.01, 115.00, 103.04	2
	46	2-Isopropylmalic acid	C ₇ H ₁₂ O ₅	175.0625	175.0612	157.05, 115.04, 113.06	2
	47	Citric acid	C ₆ H ₈ O ₇	191.0217	191.0197	145.01, 129.01, 111.00	2
	48	Oxaloglutaric acid	C ₇ H ₈ O ₇	203.0189	203.0197	141.01, 97.02, 69.03	2
	49	Homocitric acid	C ₇ H ₁₀ O ₇	205.0351	205.0354	161.04, 143.04, 117.05	2
	50	Jasmonic acid#	C ₁₂ H ₁₈ O ₃	209.1176	209.1183	165.09, 133.01, 109.03	3
	51	Tuberonic acid#	C ₁₂ H ₁₈ O ₄	225.1125	225.1127	207.10, 181.12, 163.11, 135.08	3
	52	Palmitic acid	C ₁₆ H ₃₂ O ₂	255.2314	255.2324	237.22, 211.24, 195.21, 59.01	2
	53	2-Hydroxypalmitic acid	C ₁₆ H ₃₂ O ₃	271.2274	271.2273	253.21, 227.12,	2
	54	Linolenic acid	C ₁₈ H ₃₀ O ₂	277.2165	277.2169	259.20, 233.22, 205.21, 179.25, 165.23	2
	55	alpha-Linoleic acid	C ₁₈ H ₃₂ O ₂	279.2331	279.233	261.22	2
	56	Oleic acid	C ₁₈ H ₃₄ O ₂	281.2487	281.2486	263.25, 181.21, 127.25	2
	57	Stearic acid	C ₁₈ H ₃₆ O ₂	283.2643	283.2637	265.24, 239.25, 209.22, 183.19, 171.12	2
	58	Hydroxy octadecatrienoic acid	C ₁₈ H ₃₀ O ₃	293.2112	293.2116	275.20, 223.03, 195.13, 183.13, 171.10	2
	59	Hydroxy octadecadienoic acid	C ₁₈ H ₃₂ O ₃	295.2312	295.2276	277.20, 253.02, 223.03, 167.05	2
	60	Hydroxy octadecenoic acid	C ₁₈ H ₃₄ O ₃	297.2433	297.2429	279.23, 255.12, 225.05, 127.05	2
	61	Arachidonic acid	C ₂₀ H ₃₂ O ₂	303.2326	303.2324	285.22, 269.19, 259.24, 205.12	2
	62	Dihydroxy octadecatrienoic acid	C ₁₈ H ₃₀ O ₄	309.2075	309.2069	291.19, 199.85, 179.14, 110.03	2
	63	Trihydroxy-octadecadienoic acid	C ₁₈ H ₃₂ O ₅	327.217	327.2171	299.12, 285.21, 229.14, 211.13, 171.10	2
	64	Pinellic acid#	C ₁₈ H ₃₄ O ₅	329.2329	329.2328	229.14, 211.13, 171.10	3
	65	Tuberonic acid glucoside#	C ₁₈ H ₂₇ O ₉	387.1656	387.1655	207.10, 163.11, 101.02	3
	66	Methyl tuberonic acid glucoside#	C ₁₉ H ₃₀ O ₉	401.1823	401.1817	239.12, 221.11, 207.10, 163.06	3
Amino acids	67	Phenylalanine	C ₉ H ₁₁ NO ₂	164.0732	164.0717	147.04, 120.08	2
	68	Tyrosine	C ₉ H ₁₁ NO ₃	180.0674	180.0666	163.04, 134.06	2
	69	3,4-Dihydroxyphenylalanine	C ₉ H ₁₁ NO ₄	196.0571	196.0615	181.05, 152.07	2
	70	N-acetyl phenylalanine	C ₁₁ H ₁₃ NO ₃	206.0816	206.0823	164.07, 147.04	2
	71	N-Acetyl tyrosine	C ₁₁ H ₁₃ NO ₄	222.0766	222.0772	180.06, 178.08, 163.04	2
	72	N-benzoylaspartic acid	C ₁₁ H ₁₁ NO ₅	236.0558	236.0564	218.05, 192.06, 174.05, 120.04, 115.00	2
	73	N-glucosyl ethanolamine	C ₈ H ₁₇ NO ₇	238.0927	238.0932	220.08, 202.07, 139.00	2
	74	N-Acetyl tryptophan	C ₁₃ H ₁₄ N ₂ O ₃	245.0925	245.0932	203.08, 185.07, 170.06, 116.05,	2
Terpenoids	75	Triptophenolide A1#	C ₂₀ H ₂₄ O ₃	311.1682	311.1653	295.13, 283.16, 267.17, 251.14, 237.12,	3
	76	Menthane-1,2,8,9-tetrol 2-glucoside#	C ₁₆ H ₃₀ O ₉	365.1807	365.1812	204.13, 186.12, 168.11	3

Table 5 (continued)

	No.	Compound name	EF	OM (m/z) ⁻	CM (m/z) ⁻	MS/MS (negative mode)	CL
	77	α , γ -Onoceradienedione	C ₃₀ H ₄₆ O ₂	437.3426	437.342	219.17, 205.15	2
	78	4,5-dioxo 10- <i>epi</i> -4,5- <i>seco</i> - γ -eudesmol 2'-O-acetyl-fucopyranoside#	C ₂₃ H ₃₈ O ₈	441.2508	441.2488	399.23, 253.18, 221.15, 191.14	3
	79	Oleanolic acid	C ₃₀ H ₄₈ O ₃	455.353	455.3525	407.33, 391.30, 377.28, 363.26	2
Others	80	Glucose	C ₆ H ₁₂ O ₆	179.0572	179.0561	163.06, 147.06, 115.04	2
	81	Psoralen	C ₁₁ H ₆ O ₃	185.025	185.0244	157.02, 141.03, 129.03, 115.01	2
	82	Gluconic acid	C ₆ H ₁₂ O ₇	195.0522	195.051	177.01, 151.06, 129.02, 121.04	2
	83	Ethyl glucoside	C ₈ H ₁₆ O ₆	207.0854	207.0847	179.05, 163.06, 147.06, 115.04	2
	84	Bargapten	C ₁₂ H ₈ O ₄	215.0348	215.0344	185.02, 157.02, 141.03, 129.03, 115.01	2
	85	Glucosylglycolate	C ₈ H ₁₄ O ₈	237.0619	237.0616	220.05, 207.05, 193.07, 163.06, 147.02	2
	86	Oxyresveratrol	C ₁₄ H ₁₂ O ₄	243.0656	243.0663	225.05, 199.05, 161.06, 135.04	2
	87	2-deoxy-2,3-dehydro- <i>N</i> -acetylneuraminic acid#	C ₁₁ H ₁₇ NO ₈	290.0876	290.0876	230.06, 200.05, 169.01, 128.07	3
	88	Diphyllin	C ₂₁ H ₁₆ O ₇	379.0823	379.0817	363.05, 347.01, 333.04, 319.06, 305.04	2
	89	Piceatannol glucoside	C ₂₀ H ₂₂ O ₉	405.1172	405.1178	243.06, 201.05, 159.04	2
	90	Benzyl alcohol dihexoside	C ₁₉ H ₂₈ O ₁₁	431.1564	431.1553	341.10, 269.10, 251.09, 179.05, 163.06	2
	91	Daphylloside	C ₁₉ H ₂₆ O ₁₂	445.135	445.1346	409.11, 387.12, 267.08, 179.05	2

EF. elemental formula; OM. observed mass; CM. calculated mass; CL. confidence level; (-). Negative mode. # First time identification in *Portulaca oleracea*.

in the literature (Alam et al., 2021, Islam et al., 2021, Choi et al., 2022).

3.6.3. Alkaloids

APO contains oleraceins, a type of indoline amide glycosides. Many of these compounds are glucosylated and have 5,6-dihydroxyindoline-2-carboxylic acid *N*-acylated with cinnamic acid derivatives such as hydroxybenzoyl, coumaroyl, caffeoyl, feruloyl, and sinapoyl. The following fragment ions indicate the types of hydroxy cinnamic acid *N*-linked to the indoline core, at m/z 340.08, 356.07, and 370.09 for coumaroyl, caffeoyl and feruloyl, respectively. Furthermore, oleraceins also yielded characteristic ions by neutral loss of CO (28 Da), COO (44 Da), hydroxybenzoyl (120 Da), coumaroyl (146 Da), caffeoyl (162 Da), feruloyl (176 Da), sinapoyl (206 Da), glucosyl (162 Da), double glucosyl (324 Da) and triple glucosyl (486 Da). The first oleracein compound found in this study was oleracein E (compound 30), which has the chemical formula C₁₂H₁₃NO₃ and produces a deprotonated ion at m/z 218.0833. The loss of an HCHO molecule and an HCOCH = CH₂ molecule, respectively, resulted in the production of the fragment ions with m/z 188.07 and 162.05 respectively. It also undergoes *i*-cleavage of the middle ring's phenyl and C—C connections, producing fragment ions with m/z values of 135.04 and 121.02, respectively (Fig. 3C). Moreover, compounds 36–44 were identified as oleracein U, A, B, C, I, P, N/S, L/J, and O, respectively, based on commonalities

seen between their fragmentation behaviors and those reported in the literature (Voynikov et al., 2021).

Furthermore, hydroxycinnamic acid amide yielded the base ion at m/z 147.04 (coumaroyl), m/z 163.04 (caffeoyl), m/z 177.05 (feruloyl) and m/z 207.06 (sinapoyl) by elimination of tyramine (137 Da) moiety. Further fragmentation was generated by the loss of a molecule of CO from the base peak. In addition, the tyramine moiety was further loss of NH₃ to yield ion at m/z 121 (Liu et al., 2021). On the basis of the above fragmentation behavior, compound 32–36 was identified as feruloylglycine, coumaroyltyramine, caffeoyltyramine, feruloyltyramine and feruloyloctopamine, respectively (Zhou et al., 2015).

3.6.4. Carboxylic acids, fatty acids and amino acids

From comparisons of the mass and the fragmentation behaviors of the precursor ion based on mass spectroscopic analysis reported in literature and various online databases, compounds 45–49, and 52–64 were identified as carboxylic acids, and fatty acids, respectively (Table 5). In addition, compound 67–74 were characterized as amino acids (Guijas et al., 2018, Naveja et al., 2018, Nematallah et al., 2018, Ruan et al., 2019, Islam et al., 2020, Alam et al., 2021, Najm et al., 2021, Wang et al., 2021). Furthermore, molecule 50, 51, 65, and 66 were recognized as jasmonic acid and its derivatives (tuberonic acid, tuberonic acid glucoside, and methyl tuberonic acid glucoside) based on the mass fragmentation behavior described by

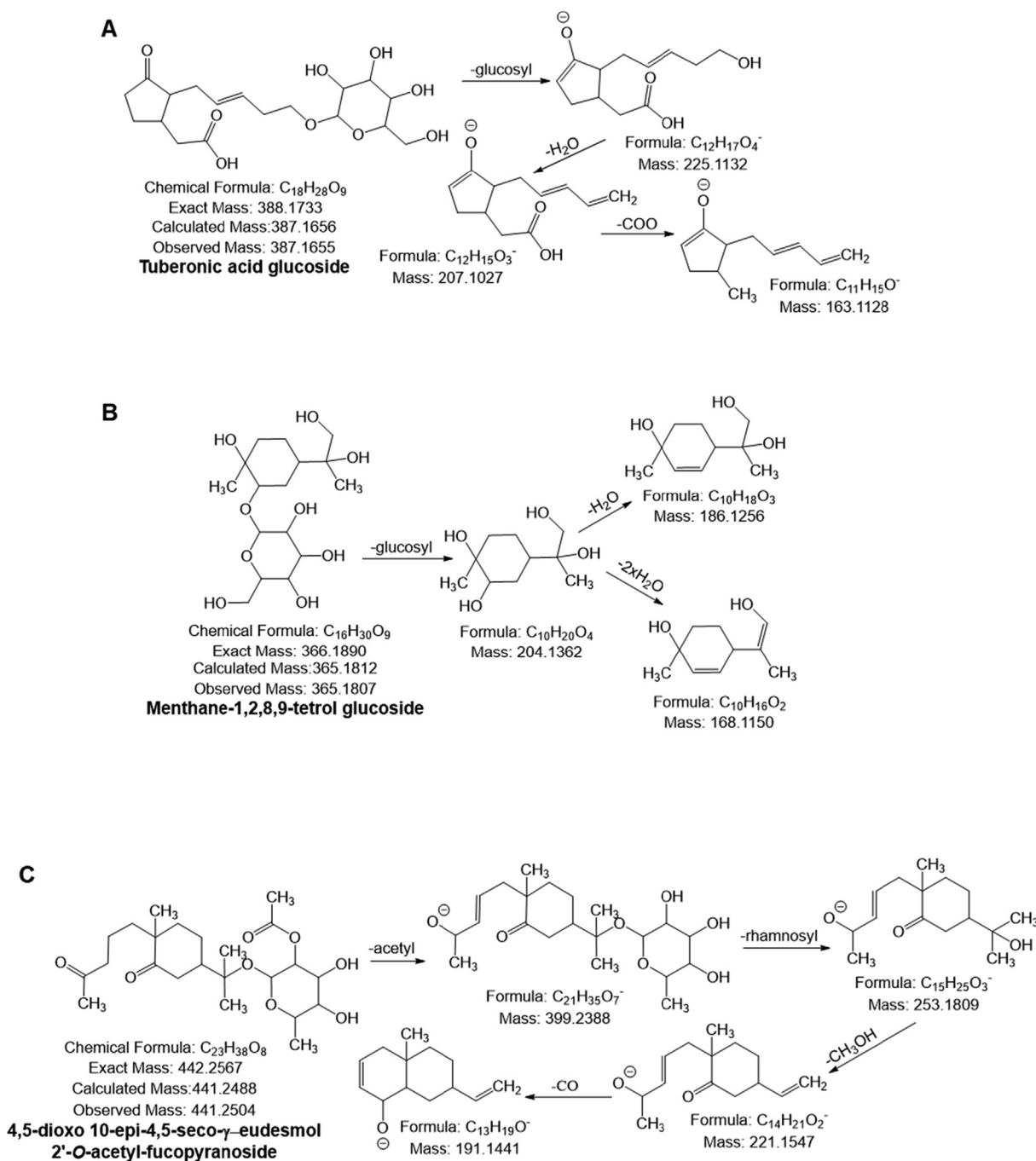


Fig. 4 Possible mass fragmentation pattern of (A) tuberonic acid glucoside, (B) menthane-1,2,8,9-tetrol glucoside and (C) 4-5-dioxo 10-epi-4,5-seco- γ -eudesmol 2'-O-acetyl-fucopyranoside.

Quirantes-Pine et al (Quirantes-Piné et al., 2010) (Fig. 4A). The jasmonic acid and its all derivatives are discovered for the first time in APO.

3.6.5. Terpenoids

For the first time in APO, compounds 75–79 were tentatively identified as terpenoids (Table 5). Compound 75 was identified as triptophenolide A1 (m/z 311.1682) with molecular formula $C_{20}H_{24}O_3$, based on the mass fragmentation behaviour described by Li et al., (Li et al., 2008). Compound 76 pro-

duced the deprotonated ion $[M-H]^-$ at m/z 365.1812, yielded a fragment ion at m/z 204.13 by losing the glucosyl (162 Da) moiety, which was followed by the loss of one and two molecules of H_2O to form the fragment ions at m/z 186.12 and 168.11, respectively. Accordingly, the compound was tentatively identified as menthane-1,2,8,9-tetrol glucoside (Fig. 4B) (Matsumura et al., 2002). Moreover, compound 78 generated a monoisotopic mass $[M-H]^-$ at m/z 441.2504, yielded fragment ions at m/z 399.23 ($[M-H-acetyl]^-$), 253.18 ($[M-H-acetyl-rhamnosyl]^-$), 221.15 ($[M-H-253.18-CH_3OH]^-$) and 191.14 ($[M-H-221.15-CO]^-$) and was tenta-

tively identified as 4,5-dioxo 10-*epi*-4,5-*seco*- γ -eudesmol 2'-*O*-acetyl-fucopyranoside with molecular formula $C_{23}H_{38}O_8$ (Fig. 4C).

3.6.6. Others

compounds 80–91 were identified as glucose (m/z 179.0572), psoralen (m/z 185.0250), gluconic acid (m/z 195.0522), ethyl glucoside (m/z 207.0854), bergapten (m/z 215.0384), glucosylglycolate (m/z 237.0619), oxyresveratrol (m/z 243.0656), 2-deoxy-2,3-dehydro-*N*-acetylneuraminic acid (m/z 290.0876), diphyllin (m/z 379.0823), piceatannol glucoside (m/z 405.1178), benzyl alcohol glucoside (m/z 431.1564) and daphylloside (m/z 445.1346), based on the similarities noticed in their fragmentation behaviors and the behaviors mentioned in the literature.

4. Conclusions

This work, which was the first investigation into optimizing the HRE conditions on APO using two modeling approaches (RSM and ANN), revealed the presence of phenolic acids, flavonoids, alkaloids, fatty acid and terpenoids, through high-resolution mass spectroscopy examination. The ANN model is more accurate and sophisticated than the RSM model, as evidenced by the fact that it had a higher R^2 and lower RMSE, AAD, and SEP values than the latter. The ideal parameters were identified as 60 % ethanol, extraction time of 90.5 min of extraction time, and 50 °C of extraction temperature. The highest values of TPC, TFC, DPPH radical scavenging effect, and ascorbic acid equivalent FRAP were found as 8.23 ± 1.06 mgGAE/g, 43.12 ± 1.15 mgCAE/g, 43.01 ± 1.25 %, and 35.98 ± 0.19 , respectively, under these circumstances. These results lead us to the conclusion that APO, a viable candidate for an antioxidant functional food, can be widely used commercially in the nutraceutical food and pharmaceutical industries.

CRedit authorship contribution statement

Fanar Alshammari: Methodology, Formal analysis, Investigation, Writing – original draft. **Md Badrul Alam:** Conceptualization, Investigation, Formal analysis, Project administration, Writing – review & editing. **Marufa Naznin:** Methodology, Investigation, Formal analysis. **Sunghwan Kim:** Conceptualization, Supervision, Writing – review & editing. **Sang-Han Lee:** Conceptualization, Methodology, Supervision, Funding acquisition, Project administration, Writing – review & editing.

Declaration of competing interest

The authors declare that they have no known competing financial interests or personal relationships that could have appeared to influence the work reported in this paper.

Acknowledgments

This study was supported by the National Research Foundation of Korea (NRF) funded by the Ministry of Science and ICT (2020R1A2C2011495 and 2021R11A1A01058062). Fanar Alshammari received the financial support for his Ph.D. studying project from Education Ministry of Kingdom of Saudi Arabia (EMSA).

Appendix A. Supplementary material

Supplementary data to this article can be found online at <https://doi.org/10.1016/j.arabjc.2022.104425>.

References

- Abdelrahman, M., Mahmoud, H., El-Sayed, M., et al, 2017. Isolation and characterization of Cepa2, a natural alliospiroside A, from shallot (*Allium cepa* L. *Aggregatum* group) with anticancer activity. *Plant Physiol. Biochem.* : PPB. 116, 167–173. <https://doi.org/10.1016/j.plaphy.2017.05.006>.
- Alam, M.B., Ju, M.K., Lee, S.H., 2017. DNA protecting activities of *Nymphaea nouchali* (Burm. f) flower extract attenuate t-BHP-induced oxidative stress cell death through Nrf2-mediated induction of Heme Oxygenase-1 expression by activating MAP-kinases. *Int. J. Mol. Sci.* 18. <https://doi.org/10.3390/ijms18102069>.
- Alam, M.B., Naznin, M., Islam, S., et al, 2021. High resolution mass spectroscopy-based secondary metabolite profiling of *Nymphaea nouchali* (Burm. f) stem attenuates oxidative stress via regulation of MAPK/Nrf2/HO-1/ROS pathway. *Antioxidants* 10, 719.
- Alam, M.B., Naznin, M., Islam, S., et al, 2021. High resolution mass spectroscopy-based secondary metabolite profiling of *Nymphaea nouchali* (Burm. f) stem attenuates oxidative stress via regulation of MAPK/Nrf2/HO-1/ROS pathway. *Antioxidants* (Basel Switzerland) 10. <https://doi.org/10.3390/antiox10050719>.
- Alam, P., Noman, O.M., Herqash, R.N., et al, 2022. Response surface methodology (RSM)-based optimization of ultrasound-assisted extraction of Sennoside A, Sennoside B, Aloe-Emodin, Emodin, and Chrysophanol from *Senna alexandrina* (Aerial Parts): HPLC-UV and antioxidant analysis. *Molecules* (Basel, Switzerland). 27. <https://doi.org/10.3390/molecules27010298>.
- Berardini, N., Carle, R., Schieber, A., 2004. Characterization of gallotannins and benzophenone derivatives from mango (*Mangifera indica* L. cv. 'Tommy Atkins') peels, pulp and kernels by high-performance liquid chromatography/electrospray ionization mass spectrometry. *Rapid Commun. Mass Spectromet.* : RCM. 18, 2208–2216. <https://doi.org/10.1002/rcm.1611>.
- Choi, H.-J., Naznin, M., Alam, M.B., et al, 2022. Optimization of the extraction conditions of *Nypa fruticans* Wurm. using response surface methodology and artificial neural network. *Food Chem.* 381. <https://doi.org/10.1016/j.foodchem.2022.132086>.
- Dadgar, M., Hosseini Varkiyani, S.M., Merati, A.A., 2015. Comparison between artificial neural network and response surface methodology in the prediction of the parameters of heat set polypropylene yarns. *J. Text. Inst.* 106, 417–430. <https://doi.org/10.1080/00405000.2014.924656>.
- David Samuel, O., Adekojo Waheed, M., Taheri-Garavand, A., et al, 2021. Prandtl number of optimum biodiesel from food industrial waste oil and diesel fuel blend for diesel engine. *Fuel* 285. <https://doi.org/10.1016/j.fuel.2020.119049>.
- Do, Q.D., Angkawijaya, A.E., Tran-Nguyen, P.L., et al, 2014. Effect of extraction solvent on total phenol content, total flavonoid content, and antioxidant activity of *Limnophila aromatica*. *J. Food Drug Anal.* 22, 296–302. <https://doi.org/10.1016/j.jfda.2013.11.001>.
- Du, Y.-K., Liu, J., Li, X.-M., et al, 2017. Flavonoids extract from *Portulaca oleracea* L. induce *Staphylococcus aureus* death by apoptosis-like pathway. *Int. J. Food Prop.* 20, S534–S542.
- Eidi, A., Mortazavi, P., Moghadam, J.Z., et al, 2015. Hepatoprotective effects of *Portulaca oleracea* extract against CCl4-induced damage in rats. *Pharm. Biol.* 53, 1042–1051. <https://doi.org/10.3109/13880209.2014.957783>.
- Fernández-Poyatos, M.D.P., Llorent-Martínez, E.J., Ruiz-Medina, A., 2021. Phytochemical composition and antioxidant activity of *Portulaca oleracea*: influence of the steaming cooking process.

- Foods (Basel, Switzerland) 10. <https://doi.org/10.3390/foods10010094>.
- Gong, X., Zhang, Y., Pan, J., et al, 2014. Optimization of the ethanol recycling reflux extraction process for saponins using a design space approach. *PLoS One* 9, e114300.
- Guijas, C., Montenegro-Burke, J.R., Domingo-Almenara, X., et al, 2018. METLIN: a technology platform for identifying knowns and unknowns. *Anal. Chem.* 90, 3156–3164. <https://doi.org/10.1021/acs.analchem.7b04424>.
- Gupta, A., Sharma, D., 2014. A survey on stock market prediction using various algorithms. *Int. J. Comput. Technol. Appl.* 5, 530–533.
- Gurtovenko, A.A., Anwar, J., 2009. Interaction of ethanol with biological membranes: the formation of non-bilayer structures within the membrane interior and their significance. *J. Phys. Chem. B* 113, 1983–1992. <https://doi.org/10.1021/jp808041z>.
- Hozayen, W., Bastawy, M., Elshafeey, H., 2011. Effects of aqueous Purslane (*Portulaca oleracea*) extract and fish oil on gentamicin nephrotoxicity in albino rats. *J. Nat. Sci.* 9, 47–62.
- Huang, S.-M., Kuo, C.-H., Chen, C.-A., et al, 2017. RSM and ANN modeling-based optimization approach for the development of ultrasound-assisted liposome encapsulation of piceid. *Ultrason. Sonochem.* 36, 112–122.
- Iranshahy, M., Javadi, B., Iranshahi, M., et al, 2017. A review of traditional uses, phytochemistry and pharmacology of *Portulaca oleracea* L. *J. Ethnopharmacol.* 205, 158–172. <https://doi.org/10.1016/j.jep.2017.05.004>.
- Islam, S., Alam, M.B., Ahmed, A., et al, 2020. Identification of secondary metabolites in *Averrhoa carambola* L. bark by high-resolution mass spectrometry and evaluation for α -glucosidase, tyrosinase, elastase, and antioxidant potential. *Food Chem.* 332. <https://doi.org/10.1016/j.foodchem.2020.127377>
- Islam, S., Alam, M.B., Ann, H.-J., et al, 2021. Metabolite profiling of *Manilkara zapota* L. leaves by high-resolution mass spectrometry coupled with ESI and APCI and in vitro antioxidant activity, α -Glucosidase, and Elastase inhibition assays. *Int. J. Mol. Sci.* 22, 132.
- Jaiswal, R., Patras, M.A., Eravuchira, P.J., et al, 2010. Profile and characterization of the chlorogenic acids in green Robusta coffee beans by LC-MS n: identification of seven new classes of compounds. *J. Agric. Food Chem.* 58, 8722–8737.
- Kachlicki, P., Piasecka, A., Stobiecki, M., et al, 2016. Structural characterization of flavonoid Glycoconjugates and their derivatives with mass spectrometric techniques. *Molecules* 21. <https://doi.org/10.3390/molecules21111494>.
- Karimi, G., Aghasizadeh, M., Razavi, M., et al, 2011. Protective effects of aqueous and ethanolic extracts of *Nigella sativa* L. and *Portulaca oleracea* L. on free radical induced hemolysis of RBCs. *Daru* 19, 295–300.
- Kumar, A., Sharma, A., Vijayakumar, M., et al, 2010. Antiulcerogenic effect of ethanolic extract of *Portulaca oleracea* experimental study. *Pharmacologyonline* 1, 417–432.
- Kusuma, H.S., Amenaghawon, A.N., Darmokoeseomo, H., et al, 2021. Evaluation of extract of *Ipomoea batatas* leaves as a green coagulant–flocculant for turbid water treatment: Parametric modelling and optimization using response surface methodology and artificial neural networks. *Environ. Technol. Innov.* 24. <https://doi.org/10.1016/j.eti.2021.102005>
- Kusuma, H.S., Amenaghawon, A.N., Darmokoeseomo, H., et al, 2022. A comparative evaluation of statistical empirical and neural intelligence modeling of *Manihot esculenta*-derived leaves extract for optimized bio-coagulation-flocculation of turbid water. *Ind. Crop. Prod.* 186. <https://doi.org/10.1016/j.indcrop.2022.115194>
- Li, R., Peng, A., He, C., et al, 2008. Analysis of triptophenolide and its related compounds from *Tripterygium wilfordii* Hook.f by electrospray ionization tandem mass spectrometry. *Int. J. Mass Spectrom.* 278, 38–49. <https://doi.org/10.1016/j.ijms.2008.08.007>.
- Liu, Y., Zheng, W., Zhong, Y., et al, 2021. Identification of α -glucosidase inhibitors from *Cortex Lycii* based on a bioactivity-labeling high-resolution mass spectrometry–metabolomics investigation. *J. Chromatogr. A* 1642, 462041.
- Llorach, R., Favari, C., Alonso, D., et al, 2019. Comparative metabolite fingerprinting of legumes using LC-MS-based untargeted metabolomics. *Food Res. Int.* (Ottawa, Ont.) 126. <https://doi.org/10.1016/j.foodres.2019.108666>
- Ma, Y., Meng, A., Liu, P., et al, 2022. Reflux extraction optimization and antioxidant activity of phenolic compounds from *Pleuroblastus amarus* (Keng) Shell. *Molecules* (Basel, Switzerland) 27. <https://doi.org/10.3390/molecules27020362>.
- Malek, F., Boskabady, M., Borushaki, M.T., et al, 2004. Bronchodilatory effect of *Portulaca oleracea* in airways of asthmatic patients. *J. Ethnopharmacol.* 93, 57–62.
- Matsumura, T., Ishikawa, T., Kitajima, J., 2002. Water-soluble constituents of caraway: carvone derivatives and their glucosides. *Chem. Pharm. Bull.* 50, 66–72. <https://doi.org/10.1248/cpb.50.66>.
- Najm, O.A., Addnan, F.H., Mohd-Manzor, N.F., et al, 2021. Identification of phytochemicals of *Phoenix dactylifera* L. Cv Ajwa with UHPLC-ESI-QTOF-MS/MS. *Int. J. Fruit Sci.* 21, 848–867. <https://doi.org/10.1080/15538362.2021.1939227>.
- Naveja, J. J., M. P. Rico-Hidalgo and J. L. Medina-Franco, 2018. Analysis of a large food chemical database: chemical space, diversity, and complexity. *F1000Research*. 7, Chem Inf Sci-993. <https://doi.org/10.12688/f1000research.15440.2>.
- Nayaka, H., Londonkar, R.L., Umesh, M., 2014. Evaluation of potential antifertility activity of total flavonoids, isolated from *Portulaca oleracea* L on female albino rats. *Int. J. PharmTech. Res.* 6, 783–793.
- Nematallah, K.A., Ayoub, N.A., Abdelsattar, E., et al, 2018. Polyphenols LC-MS2 profile of Ajwa date fruit (*Phoenix dactylifera* L.) and their microemulsion: potential impact on hepatic fibrosis. *J. Funct. Foods* 49, 401–411. <https://doi.org/10.1016/j.jff.2018.08.032>.
- Okwu, M.O., Samuel, O.D., Otanocha, O.B., et al, 2020. Development of ternary models for prediction of biogas yield in a novel modular biodigester: a case of fuzzy Mamdani model (FMM), artificial neural network (ANN), and response surface methodology (RSM). *Biomass Convers. Biorefin.* <https://doi.org/10.1007/s13399-020-01113-1>.
- Okwu, M.O., Samuel, O.D., Ewim, D.R.E., et al, 2021. Estimation of biogas yields produced from combination of waste by implementing response surface methodology (RSM) and adaptive neuro-fuzzy inference system (ANFIS). *Int. J. Energy Environ. Eng.* 12, 353–363. <https://doi.org/10.1007/s40095-021-00381-5>.
- Okwu, M.O., Tartibu, L.K., Samuel, O.D., et al, 2021. Predictive ability of Response Surface Methodology (RSM) and artificial Neural Network (aNN) to approximate Biogas Yield in a Modular Biodigester. Springer International Publishing.
- Pandey, D., Banik, R., 2012. Optimization of extraction conditions for colchicine from *Gloriosa superba* tubers using response surface methodology. *J. Agric. Technol.* 8, 1301–1315.
- Parveen, I., Threadgill, M.D., Hauck, B., et al, 2011. Isolation, identification and quantitation of hydroxycinnamic acid conjugates, potential platform chemicals, in the leaves and stems of *Miscanthus × giganteus* using LC–ESI-MSn. *Phytochemistry* 72, 2376–2384.
- Petropoulos, S., Karkanis, A., Martins, N., et al, 2016. Phytochemical composition and bioactive compounds of common purslane (*Portulaca oleracea* L.) as affected by crop management practices. *Trends Food Sci. Technol.* 55, 1–10.
- Quirantes-Piné, R., Arráez-Román, D., Segura-Carretero, A., et al, 2010. Characterization of phenolic and other polar compounds in a lemon verbena extract by capillary electrophoresis-electrospray ionization-mass spectrometry. *J. Sep. Sci.* 33, 2818–2827. <https://doi.org/10.1002/jssc.201000228>.

- Ruan, J., Yan, J., Zheng, D., et al, 2019. Comprehensive chemical profiling in the ethanol extract of *Pluchea indica* aerial parts by liquid chromatography/mass spectrometry analysis of its silica gel column chromatography fractions. *Molecules* (Basel, Switzerland) 24. <https://doi.org/10.3390/molecules24152784>.
- Saha, J., Biswas, A., Chhetri, A., et al, 2011. Response surface optimisation of antioxidant extraction from kinema, a *Bacillus*-fermented soybean food. *Food Chem.* 129, 507–513. <https://doi.org/10.1016/j.foodchem.2011.04.108>.
- Sakai, N., Inada, K., Okamoto, M., et al, 1996. Portulacide A, a monoterpene glucoside, from *Portulaca oleracea*. *Phytochemistry* 42, 1625–1628.
- Samuel, O.D., Emovon, I., 2018. The development of expeller for kernel based seed and its oil characterization. *Int. J. Integr. Eng.* 10.
- Samuel, O.D., Okwu, M.O., 2019. Comparison of Response Surface Methodology (RSM) and Artificial Neural Network (ANN) in modelling of waste coconut oil ethyl esters production. *Energy Sources Part A* 41, 1049–1061. <https://doi.org/10.1080/15567036.2018.1539138>.
- Schymanski, E.L., Jeon, J., Gulde, R., et al, 2014. Identifying small molecules via high resolution mass spectrometry: communicating confidence. *Environ. Sci. Tech.* 48, 2097–2098. <https://doi.org/10.1021/es5002105>.
- Sedraoui, S., Badr, A., Barba, M.G.M., et al, 2020. Optimization of the ultrahigh-pressure-assisted extraction of phenolic compounds and antioxidant activity from palm dates (*Phoenix dactylifera* L.). *Food Anal. Methods* 13, 1556–1569. <https://doi.org/10.1007/s12161-020-01764-w>.
- Sodeifian, G., Ardestani, N.S., Sajadian, S.A., et al, 2018. Properties of *Portulaca oleracea* seed oil via supercritical fluid extraction: experimental and optimization. *J. Supercrit. Fluids* 135, 34–44.
- Stroescu, M., Stoica-Guzun, A., Ghergu, S., et al, 2013. Optimization of fatty acids extraction from *Portulaca oleracea* seed using response surface methodology. *Ind. Crop. Prod.* 43, 405–411.
- Tang, W., Chen, J., Du, M., et al, 2020. Analysis of chemical constituents in *Ficus Hirta* Vahl. by LCMS-IT-TOF and GC-MS. *IOP Conf. Ser.: Mater. Sci. Eng.* 730. <https://doi.org/10.1088/1757-899x/730/1/012027> 012027.
- Voynikov, Y., Nediakov, P., Gevrenova, R., et al, 2021. UHPLC-Orbitrap-MS tentative identification of 51 Oleraceins (Cyclo-Dopa Amides) in *Portulaca oleracea* L. cluster analysis and MS(2) filtering by mass difference. *Plants* (Basel Switzerland) 10. <https://doi.org/10.3390/plants10091921>.
- Vukics, V., Guttman, A., 2010. Structural characterization of flavonoid glycosides by multi-stage mass spectrometry. *Mass Spectrom. Rev.* 29, 1–16. <https://doi.org/10.1002/mas.20212>.
- Wang, W., Gu, L., Dong, L., et al, 2007. Protective effect of *Portulaca oleracea* extracts on hypoxic nerve tissue and its mechanism. *Asia Pac. J. Clin. Nutr.* 16, 227.
- Wang, C., Li, Y., Yao, L., et al, 2014. Optimization of ultrasonic-assisted extraction of flavonoid from *Portulaca oleracea* L. by response surface methodology and chemical composition analysis. *J. Korean Soc. Appl. Biol. Chem.* 57, 647–653.
- Wang, F., Ligand, J., Tian, S., et al, 2021. CFM-ID 4.0: more accurate ESI-MS/MS spectral prediction and compound identification. *Anal. Chem.* 93, 11692–11700. <https://doi.org/10.1021/acs.analchem.1c01465>.
- Xi, J., Wang, B., 2013. Optimization of ultrahigh-pressure extraction of polyphenolic antioxidants from green tea by response surface methodology. *Food Bioproc. Tech.* 6, 2538–2546. <https://doi.org/10.1007/s11947-012-0891-9>.
- Xiang, L., Xing, D., Wang, W., et al, 2005. Alkaloids from *Portulaca oleracea* L. *Phytochemistry* 66, 2595–2601.
- Yan, J., Sun, L.-R., Zhou, Z.-Y., et al, 2012. Homoisoflavonoids from the medicinal plant *Portulaca oleracea*. *Phytochemistry* 80, 37–41.
- Zadhossein, S., Abbaspour-Gilandeh, Y., Kaveh, M., et al, 2021. Exergy and energy analyses of microwave Dryer for Cantaloupe slice and prediction of thermodynamic parameters using ANN and ANFIS algorithms. *Energies* 14, 4838.
- Zhou, Y. X., H. L. Xin, K. Rahman, et al., 2015. *Portulaca oleracea* L.: a review of phytochemistry and pharmacological effects. *BioMed research international.* 2015, 925631. <https://doi.org/10.1155/2015/925631>.
- Zhu, K.-X., Lian, C.-X., Guo, X.-N., et al, 2011. Antioxidant activities and total phenolic contents of various extracts from defatted wheat germ. *Food Chem.* 126, 1122–1126. <https://doi.org/10.1016/j.foodchem.2010.11.144>.